

Full Length Article

Rapamycin improves bone mass in high-turnover osteoporosis with iron accumulation through positive effects on osteogenesis and angiogenesis

Jiadong Wu^{a,b,1}, Aifei Wang^{a,1}, Xiao Wang^a, Guangfei Li^a, Peng Jia^a, Guangsi Shen^a, Bin Chen^a, Ye Yuan^a, Hui Zhang^a, Fan Yang^{a,c}, Youjia Xu^{a,c,*}

^a Department of Orthopedics, Second Affiliated Hospital of Soochow University, 215004 Suzhou, China

^b Department of Orthopedics, Affiliated Yancheng Hospital of Southeast University Medical College, 224005 Yancheng, China

^c Osteoporosis Institute, Soochow University, 215004 Suzhou, China



ARTICLE INFO

Keywords:

Osteoporosis
Rapamycin
Iron accumulation
Osteogenesis
Angiogenesis

ABSTRACT

Iron accumulation is an independent risk factor for type I osteoporosis, but the molecular mechanisms of the phenomenon are not well defined, and effective therapy has not been reported. Here, we found that the level of mTOR was increased both in wild-type mouse models with iron accumulation and transgenic mouse models (Hepc^{-/-}) of high-turnover osteoporosis with iron accumulation. We show that an increased level of mTOR can depress osteogenesis and angiogenesis by Cxcl9 both in bone and in vitro. Suppression of mTOR in mouse models by rapamycin and in vitro by siRNA transfection recovered both osteogenesis and angiogenesis. These findings revealed the role of mTOR in osteogenesis and angiogenesis in high-turnover osteoporosis with iron accumulation and showed that rapamycin targeting of mTOR ameliorates osteogenesis and angiogenesis to improve bone mass.

1. Introduction

Osteoporosis is the one of the most prevalent metabolic bone disorders among older individuals, characterized by low bone mass, deterioration of microstructure, and increasing potential of bone fracture [1,2]. Bone metabolism and homeostasis are maintained by the balance between bone remodelling activities of osteoblasts (OBs) and osteoclasts (OCs). Decreasing activity of osteoblasts leads to osteoporosis, and crosstalk between osteogenesis and angiogenesis has been shown to play a vital role in bone regeneration [3–6]. Osteoporosis often results in a fractured hip or spine, which can be painful, inconvenient, damaging, and even fatal [7,8]. The International Osteoporosis Foundation estimates that osteoporosis affects > 200 million individuals, and osteoporosis is the most age-related bone disease worldwide, especially in postmenopausal women [9,10]. Due to the continued growth of the aging population, the number of patients with osteoporosis is sharply increasing, and osteoporosis places a significant burden not only on public health but also on the economy [11]. However, the current therapies for osteoporosis are stagnant for individual differences. Thus, identification of new pathways and acute therapies is urgently needed.

Iron accumulation, as an independent risk factor for osteoporosis, can significantly accelerate the loss of bone mass in osteoporosis, especially

in postmenopausal women [12,13]. Iron is an essential metallic element in human physiological processes [14]. Recent case reports and clinical studies have revealed that primary or secondary iron accumulation is always accompanied by osteoporosis in bone, and the level of ferritin increases with age in osteoporosis of postmenopausal women [15,16]. Moreover, the osteoporosis bone phenotype has been demonstrated in various animal models with iron accumulation, including mice and zebrafish, emphasizing the essential role of iron accumulation in osteoporosis [17]. Nevertheless, the mechanism of this phenomenon remains unclear. Balogh et al. suggested that iron accumulation has negative influence not only on the differentiation but also on the activity and extracellular matrix mineralization of mature osteoblasts [18]. Liang W et al. reported that impaired H type vessels in ovariectomized mice can be partially rescued by injection of deferoxamine, an iron chelator [19]. Crosstalk between osteogenesis and angiogenesis plays a vital role in high-turnover type osteoporosis with iron accumulation [20–22], but the complete mechanism is still unknown.

Rapamycin effectively inhibits the proliferation of yeast initially extracted from Easter Island soil samples [23]. Mammalian target of rapamycin (mTOR) is an evolutionary conserved serine/threonine kinase and exists in two structurally distinct complexes as follows: mTOR complex 1 (mTORC1) and mTOR complex 2 (mTORC2). mTORC1 is

* Corresponding author at: Department of Orthopedics, The Second Affiliated Hospital of Soochow University, Suzhou 215004, China.

E-mail address: xuyoujia@suda.edu.cn (Y. Xu).

¹ These authors contributed equally to this work.

sensitive to rapamycin, while mTORC2 is not sensitive to rapamycin [24,25]. The function of mTOR is to direct organismal growth and homeostasis by controlling cellular processes, including protein synthesis, metabolism and autophagy [26]. mTOR is recognized as a common effector that is involved in bone-related signalling, such as WNT and BMP signalling, and mTOR inhibition has beneficial effects on improving osteoporosis [27–29]. Impairment of mTOR function can suppress the differentiation and proliferation of osteoclasts and inhibit bone resorption to increase bone mass [30]. A recent study has reported that mTOR plays a vital role in the crosstalk between osteogenesis and angiogenesis [31]. These findings indicate that there is a relationship between mTOR and bone regeneration. However, there are no reports on the role of mTOR in the process of iron accumulation-induced severe bone loss in osteoporosis.

The present study found that both wild-type mice with iron accumulation and transgenic (Hepc^{-/-}) mice with high-turnover type osteoporosis with iron accumulation demonstrated enhanced levels of mTOR and that the bone masses of these mice were significantly lower than those in the control group. Rapamycin was used to suppress activated mTOR in high-turnover type osteoporosis with iron accumulation, which resulted in partial rescue of impaired bone mass and osteogenic activity, and rapamycin also partly recovered the damaged angiogenesis. Mechanistically, iron accumulation activated mTOR and enhanced the binding of signal transducer and activator of transcription 1 (STAT1) to the promoter of chemokine ligand 9 (Cxcl9) in osteoblasts. The increased Cxcl9, as a competitive inhibitor of vascular endothelial growth factor (VEGF), decreased the phosphorylation of VEGFR2 (receptor of VEGF (KDR)) both in osteoblasts and human umbilical vein endothelial cells (HUVECs), resulting in suppression of osteogenesis and angiogenesis. Thus, our study identified that mTOR plays a vital role in high-turnover osteoporosis with iron accumulation, supporting rapamycin targeting of mTOR as a novel therapy for high-turnover osteoporosis with iron accumulation.

2. Materials and methods

2.1. Animals

Wild type (Wt) and hepcidin knockout (Hepc^{-/-}) mice were obtained from the Cambridge-Soochow University Genome Resource Centre (CAM-SU GRC). The mice had a C57Bl/6 background and were housed in a specific pathogen-free (SPF) laboratory in Soochow University. The external conditions, such as temperature, ventilation, and illumination, were controlled. All animal experiments were performed in accordance with the Guide for the Care and Use of Laboratory Animals of the National Institutes of Health. Eight-week-old Wt male mice (C57/BL6, n = 10) were treated intraperitoneally three times a week for 2 months with 40 mg/kg ferric ammonium citrate (FAC; Sigma-Aldrich, #F5879, Japan) to produce iron accumulation models (Wt + FAC), while the other ten Wt male mice received intraperitoneal injections of physiological saline to produce placebo models (Wt + Saline) [32]. Eight-week-old transgenic female mice (Hepc^{-/-}, n = 10) were ovariectomized (OVX) to produce osteoporosis models with iron accumulation (Δ Hep + OVX), and the Wt female mice (n = 10) were ovariectomized to produce osteoporosis models without iron accumulation (Wt + OVX). For further study, the ovariectomized operation was performed on 16 8-week-old Wt female mice (Wt + OVX) and 48 transgenic female mice (Hepc^{-/-}). Among the transgenic female mice, 16 were treated intraperitoneally with 3 mg/kg/day rapamycin (Sigma-Aldrich, #V900930, Japan) for 2 months (Δ Hep + OVX + Rapa), which was diluted in 0.2% carboxymethyl cellulose (CMC) [33]. In addition, 16 transgenic female mice were treated with CMC as vehicle (Δ Hep + OVX + CMC), and the remaining 16 transgenic female mice were left untreated as the sham control (Δ Hep + OVX). All mice were sacrificed after the last treatment. Blood was extracted and then centrifuged at 3500g for 15 min to

obtain serum. The femur and tibia were dissected, and the soft tissue was removed and used for relative assays.

2.2. Micro-CT scanning

Femur samples were analysed by a SkyScan 1172 high-resolution micro-CT scanner (SkyScan, Belgium) with 9 μ m resolution, 50 kV, 500 μ A, and 0.5° rotation step. Trabecular regions of interest were defined from a point of approximately 540 μ m proximal to the end of the distal growth plate over 1.35 mm towards the diaphysis. Cortical regions of interest were outlined at femoral middle-diaphysis from a point of approximately 4.59 mm proximal to the end of the distal growth plate over 900 μ m towards the diaphysis. The following parameters were tested: bone mineral density (BMD; g/cm³), bone volume/total volume (BV/TV; %), trabecular number (Tb.N; 1/mm), trabecular thickness (Tb.Th; mm), trabecular separation (Tb.Sp; mm), structure model index (SMI), connectivity density (ConnD; 1/mm³), cortical bone volume (mm³), cortical bone surface (mm²), and cortical bone thickness (mm).

2.3. Prussian blue staining of bone

Undecalcified femur tissues were embedded in resin. Sections (6 μ m thick) were cut by a heavy-duty sliding microtome equipped with 40 tungsten carbide knives (Leica SM2500, German). The working fluid was a mixture of distilled water and potassium cyanide, containing concentrated hydrochloric acid. Bone sections were rinsed at 37 °C for 5 min and then incubated with working fluid at 37 °C for 30 min. The sections were incubated for 24 h at room temperature and then rinse at 37 °C for 5 min. The bone sections were sealed with neutral gum and analysed with a microscope.

2.4. Bone iron concentration

The femur samples were soaked with deionized water for two hours, incubated in 5% acetic acid for 15 min, and soaked with deionized water to remove shallow metal ions. Samples were then incubated in 10% hydrogen peroxide for 4 h, and samples were then incubated in anhydrous alcohol and subjected to ultrasound for 5 min. After 30 min of soaking, the soft tissue and fat were removed. After washing and transferring to a clean conical bottle, bone tissues were dried in an 85 °C oven. Specimens were weighed accurately and digested in using a microwave. Inductively coupled plasma mass spectrometry (ICP-MS, China) was used to analyse the bone iron concentration relative to the dry weight of femur.

2.5. Scanning electron microscope (SEM)

Femur specimens were cleaned with phosphate buffered saline (PBS) and fixed with glutaraldehyde for 3 h. Specimens were then washed three times with PBS (15 min each time) and fixed with osmium acid for 1 h. Specimens were washed with different concentrations of tert-butyl alcohol (30%, 50%, 70%, 80%, 90% and 100%) and then subjected to dessication and sprayed with gold. SEM (EVO18, Germany) was used to analyse and photograph the microstructure of the distal femur at high magnification (\times 300).

2.6. Biomechanical testing

An electronic universal experimental machine (WDW-4100, Soochow University) was used for the three point bending test of the femur. The long and short diameters of the femoral shaft were measured with a Vernier calliper, and specimens were then placed between two support abutments. The load was applied to middle of the femoral shaft through a touching probe. During this test, the posterior surface was in tension, and the anterior surface was in compression. The

strength variables (bending modulus of elasticity, bending energy, maximum bending stress and bending rigidity coefficient) were calculated with a standard engineering formula [34].

2.7. Cell culture and treatment

The hFOB1.19 osteoblast cell line was purchased from Procell Life Science & Technology. The cells were cultured according to the procedures of American Type Culture Collection (Manassas). hFOB1.19 cells were maintained in α -MEM (HyClone, #SH30265.01, US) supplemented with 10% foetal bovine serum (FBS; Biological Industries, #04-001-1A, US) and 0.3 g/L G418 (Sigma Aldrich, #345810, Japan), and they were cultured in a humidified incubator with 5% CO₂ at 33.4 °C. The medium was replaced twice a week, and the cells were cultured using Trypsin-EDTA solution (Beyotime Institute of Biotechnology, #C0201, China). Human BM-MNCs (1×10^6 cells/well) were cultured with human M-CSF (25 ng/ml; from day 0) plus recombinant soluble RANKL (receptor activator of nuclear factor kappa B (NF- κ B) ligand) (50 ng/ml; from day 3) in α -MEM supplemented with 10% fetal bovine serum (FBS), 100 units/ml penicillin and 100 mg/ml streptomycin, in 24 well plates under 5% CO₂ at 37 °C. FAC (Sigma-Aldrich, #F5879, Japan), an iron-related donor, was used to simulate an iron accumulation environment in vitro. hFOB1.19 cells and BM-MNCs were incubated with 200 μ M FAC, and control groups were treated with PBS. After exposure to FAC for 24 h, all samples were collected for relative assays. HUVECs were purchased from Procell Life Science & Technology. HUVECs were maintained in DMEM (HyClone, #SH30243.01, US) culture medium containing 10% foetal bovine serum (FBS; Biological Industries, #04-001-1A US), and they were cultured in a humidified incubator with 5% CO₂ at 37 °C. The medium was replaced three times a week, and the cells were lifted using Trypsin-EDTA solution (Beyotime Institute of Biotechnology, #C0201, China). Adherent HUVECs were incubated with corresponding medium extracted from treated osteoblasts for 48 h, and all samples were then collected for relative assays.

2.8. siRNA knockdown

hFOB1.19 cells were transiently transfected with negative control and mTOR siRNA using Lipofectamine RNAi 2000 (Invitrogen, #11668030, US) in Opti-MEM medium (Gibco, #31985062, US) according to the manufacturer's instructions. The efficiency of transfection was measured by western blotting. The sequence of the mTOR siRNA was as follows: forward, 5'-CCACCCGAAUUGGCAGAUUTT-3' and reverse, 5'-AAUCUGCCAAUUCGGUGGTT-3' (GenePharma, China).

2.9. Cell proliferation assay

Cells were seeded (103 cells per well) in 96-well plates. After cells were treated for 24 h, a solution containing fresh medium (90 μ l) and CCK-8 reactant (10 μ l) (Dojindo, #CK04, Japan) was added to each well, and cells were incubated at 37 °C for 2 h in the dark followed by addition of stop buffer. Absorbance at 450 nm was then measured using an enzyme-labelled instrument (Thermo, US). All operations were performed in accordance with the manufacturer's instructions.

2.10. Staining of alkaline phosphatase (ALP)

hFOB1.19 cells cultured on 12-well plates were rinsed thrice with PBS, fixed in 4% paraformaldehyde (PFA) for 15–30 min, washed twice with PBS and incubated with a solution of *p*-nitrophenyl phosphate from the Alkaline Phosphatase Assay Kit (Beyotime Institute of Biotechnology, #C3206, China) at room temperature in the dark for 2 h according to the manufacturer's instructions, and it's all same to tibias' sections of all groups.

2.11. Staining of Alizarin Red

hFOB1.19 cells cultured on 12-well plates were washed twice with PBS (calcium and magnesium free), fixed in 4% PFA for 15–30 min and washed twice with PBS (calcium and magnesium free). Calcium deposits in osteoblasts were detected by the Alizarin Red S Staining Kit (Solarbio, #G3280, China) according to the manufacturer's instructions.

2.12. Staining of tartrate resistant acid phosphatase (TRAP)

Osteoclasts induced from BMNCs (Bone marrow mononuclear cells) were washed twice with PBS (calcium and magnesium free), fixed in 4% PFA for 15–30 min and washed twice with PBS. TRAP+ cells were detected by the TRAP kit (Sigma-Aldrich, #378A-1k, Japan). All operations were performed in accordance with the manufacturer's instructions, and it's all same to tibias' sections of all groups.

2.13. In vitro migration assays

HUVECs were seeded (1×10^5 cells per well) in 24-well plates (Corning, US). A linear wound was created in monolayers by scratching with a sterile pipette tip (200 μ l yellow tip). Monolayers were washed with PBS to remove floating cells, and the corresponding medium was added. After an additional 24 h, cell migration into the wound was assessed by microscopy using a digital inverted microscope. The degree of wound closure was measured as the percentage of the area covered by migrating cells in the initial wound in eight wounds per test condition using ImageJ software.

2.14. In vitro tube formation assay

HUVECs were seeded at a density of 1×10^5 per well in 24-well plates with growth factor-depleted Matrigel (Corning, #356234, US). Conditional medium was added, and the results were quantified 10 h later. Microscopic fields containing the tube structures formed in the gel were photographed at low magnification ($\times 4$). Before the HUVECs were imaged, they were fixed with 4% PFA. Tube area was quantified with ImageJ software.

2.15. Collection of corresponding medium of hFOB1.19 cells

Twenty-four hours after seeding cells on 6 cm² plates, the corresponding medium of hFOB1.19 cells was collected and stored at –80 °C.

2.16. Western blot assays

Bone samples were ground into powder with the liquid nitrogen and then lysed using RIPA solution containing protease inhibitor (Roche, #4693132001, CH) on ice for 30 min. Lysates were centrifuged, and supernatants were collected. Cells were washed with PBS and then lysed using RIPA solution containing protease inhibitor on ice for 30 min. Cell lysates centrifuged, and the supernatants were then collected. The collected supernatants were separated by SDS-polyacrylamide gel electrophoresis and blotted onto transfer membranes (Immobilon, #IPVH00010, US). Membranes were then incubated with the following specific antibodies: mTOR (Abcam, #2983, UK); Slit3 (R&D Systems, #AF3629, US); STAT1 (Proteintech, #10144-2-AP, US); VEGF (Proteintech, #19003-1-AP, US); Cxcl9 (R&D, #MAB392, US); KDR (ABclonal, #A7695, China); P-KDR (ABclonal, #AP0382, China); Runx2 (Bioworld Technology, #BS8734, US); and OCN (Santa Cruz Biotechnology, #sc-365797, US). The membranes were visualized with a solution of 100 mM Tris-HCl, luminal, 30% H₂O₂, and coumaric acid.

Abbreviations: mTOR, mammalian target of rapamycin; Slit3, slit guidance ligand 3; STAT1, signal transducer and activator of

transcription 1; Cxcl9, chemokine ligand 9; VEGF, vascular endothelial growth factor; KDR (VEGFR2), receptor of VEGF; P-KDR, phosphorylation of KDR; Runx2: Runt-related transcription factor 2; OCN: Osteocalcin.

2.17. Real-time quantitative PCR

Bone samples were ground using liquid nitrogen, and total RNA was obtained by TRIzol Reagent (Invitrogen, #15596018, US). RNA was reversed transcribed with the PrimeScript Reverse Transcriptase Kit according to the manufacturer's protocol (Takara, #RR047A, Japan). cDNA (2 µg) was used for real-time PCR using SYBR Premix Ex Taq (Takara, #RR420A, Japan). The following primers for mouse *mTOR*, *Runx2*, *SP7*, *ALP*, *Slit3*, *VEGF*, *STAT1* and *Cxcl9* and human *mTOR*, *Runx2*, *OCN*, *ALP*, *STAT1*, *VEGF*, *Cxcl9* and *KDR* were used: mouse *mTOR* forward, 5'-ACCGGCACACATTGAAGAAG-3' and reverse, 5'-CTCGTTGAGGATCAGCAAGG-3'; mouse *Runx2* forward, 5'-GACTGTGGTTACCGTCATGGC-3' and reverse, 5'-GCCACAAAATCTCAGATC GTT-3'; mouse *SP7* forward, 5'-AGCCTGCAGCAAATTTGG-3' and reverse, 5'-TGAAAGGTCAGCGTATGGCTT-3'; mouse *ALP* forward, 5'-CAGCGGGTAGGAAGCAGTTTC-3' and reverse, 5'-CCCTGCACCTCA TCCCTGA-3'; mouse *Slit3* forward, 5'-TGCCCCACCAAGTGTACCT-3' and reverse, 5'-GGCCAGCGAAGTCCATTTG-3'; mouse *VEGF* forward, 5'-GAGGTCAAGGCTTTGAAGGC-3' and reverse, 5'-CTGTCTGGTAT TGAGGTTGG-3'; mouse *STAT1* forward, 5'-TCACAGTGGTTCGAGCTT CAG-3' and reverse, 5'-GCAAACGAGACATCATAGGCA-3'; mouse *Cxcl9* forward, 5'-GGAGTTCGAGGAACCCCTAGTG-3' and reverse, 5'-GGGATT TGTAGTGGATCGTGC-3'; human *mTOR* forward, 5'-ATGCCACCACCC TCATAGAT-3' and reverse, 5'-CTGGGTTCCAGACTGCTAG-3'; human *Runx2* forward, 5'-TGGTACTGTCTATGGCGGGTA-3' and reverse, 5'-TCTCAGATCGTTGAACCTTGCTA-3'; human *OCN* forward, 5'-CACT CCTCGCCTATTGGC-3' and reverse, 5'-CCCTCTGCTTGGACACA AAG-3'; human *ALP* forward, 5'-ACCACCAGAGAGTGAACCA-3' and reverse, 5'-CGTTGTCTGAGTACCAGTCCC-3'; human *STAT1* forward, 5'-ATCAGGCTCAGTCGGGGAATA-3' and reverse, 5'-TGGTCTCGTGT CTCTGTTCT-3'; human *VEGF* forward, 5'-AGGGCAGAATCATCACGA AGT-3' and reverse, 5'-AGGGTCTCGATTGGATGGCA-3'; human *Cxcl9* forward, 5'-CCTTAAACAATTTGCCCAA-3' and reverse, 5'-TCACATCT GCTGAATCTGGG-3'; and human *KDR* forward, 5'-GGCCCAATAATCA GAGTGGCA-3' and reverse, 5'-CCAGTGTCAATTCGGATCACTTT-3'.

2.18. ELISA assays

The levels of mTOR, ferritin, ALP, PINP and osteocalcin in serum were detected using the following ELISA kits: mTOR ELISA Kit (Abcam, #ab206311, UK); Ferritin ELISA Kit (Abnova, #KA1941, China); ALP ELISA Kit (CUSABIO, #E11914m, US); PINP ELISA Kit (Cloud-Clone corp, #SEA957Mu, US); and Osteocalcin ELISA Kit (Cloud-Clone corp, #SEA471Mu, US). A human Cxcl9 ELISA kit (Abcam, #ab119588, UK) was used to analyse the Cxcl9 level in the medium of treated hFOB1.19 cells. All the procedures were performed according to the manufacturers' instructions.

2.19. Iron concentration of culture medium from osteoblasts

The Iron assay kit (Abcam, #ab83366, UK) was used to analyse the iron concentration in the culture medium of treated osteoblasts according to the manufacturers' instructions.

2.20. Immunostaining of sections and cells

The tibias of mice were decalcified with 5% EDTA at 4 °C for 2 months, embedded in OCT (Sakura, #25608930, Japan) at -20 °C for 12 h and then sectioned using a freezing microtome (Leika CM1520, DE). Tibia sections were washed thrice with PBST, blocked with 5% BSA for 30 min and then incubated with primary antibodies. The

following primary antibodies were used: mouse EMCN (Santa Cruz, #sc-19901, US); mouse CD31 (R&D, #FAB3628G-025, US); human EMCN (Abcam, #ab45771, UK); and human CD31 (Dako, #M0823, US). The processed sections were visualized and imaged using a Multiphoton Laser Scanning Microscope (Olympus, Japan). Treated cells were washed with PBS, fixed using 4% PFA in PBS for 15 min, washed thrice with PBS and blocked with 5% BSA in PBS for 30 min. Subsequently, cells were incubated with primary antibody overnight at 4 °C and then incubated with fluorescence-conjugated secondary antibodies at room temperature in the dark for 1 h. A Multiphoton Laser Scanning Microscope (Olympus, Japan) was used for imaging.

2.21. Statistical analysis

The quantitative data are expressed as the mean ± standard deviation (SD). Student's *t*-test and One-way ANOVA followed by Bonferroni post-tests was used for the comparison analysis using SPSS 21.0 software. *P* < 0.05 was considered statistically significant.

3. Results

3.1. Iron accumulation activates osteoblastic mTOR

Iron accumulation significantly inhibits the proliferation and differentiation of osteoblasts [17,35]. As the proliferation and differentiation of osteoblasts is tightly related to mTOR, the effect of iron on mTOR in osteoblasts was determined. To generate the mouse models with iron accumulation, FAC was intraperitoneally injected into male mice. The FAC-treated mice showed increased serum ferritin compared to the control group (Fig. 1A). Consistently, both the iron concentration and Prussian blue staining of bone showed increased deposition of iron in bone (Fig. 1B–C), indicating that the mouse models with iron accumulation were effectively established. Interestingly, serum mTOR levels in these mice were significantly enhanced, and the mTOR protein and mRNA expression levels in bone were clearly higher than those in the control group (Fig. 1D–F). These findings suggested that iron accumulation activates mTOR in vivo.

For in vitro analysis, osteoblasts were treated with FAC, and the concentration of FAC was determined by the CCK-8 kit (Supplementary Fig. 1). A higher concentration of iron in culture medium was confirmed by the iron assay kit (Fig. 1G). Consistent with the in vivo results, both mTOR protein and mRNA expression levels were enhanced by iron in osteoblasts (Fig. 1H–I). Together, these data indicated that iron accumulation promotes the expression of mTOR in vivo and in vitro.

3.2. Endogenous iron accumulation activates mTOR in bone of high-turnover osteoporosis

Because iron accumulation induced the activation of mTOR in wild-type mice, the relationship between iron accumulation and mTOR in mice with osteoporosis was investigated. To generate mouse models of high-turnover osteoporosis with endogenous iron accumulation, 8-week-old *Hepc*^{-/-} female mice were ovariectomized and compared to ovariectomized 8-week-old Wt female mice. After two months, *Hepc*^{-/-} female mice showed increased iron deposition via Prussian blue staining of liver, and there was no difference in body weight (Supplementary Fig. 2). Moreover, *Hepc*^{-/-} female mice had a markedly higher ferritin level than wild-type mice, and the iron concentration and Prussian blue staining of bone showed consistent variety (Fig. 2A–C). Micro-computed tomography (micro-CT) analysis revealed the decreased volume of trabecular bone and lower BMD in *Hepc*^{-/-} mice with ovariectomy (Fig. 2D–E). All these data indicated that endogenous iron accumulation in mice of high-turnover type osteoporosis is induced with successful hepcidin knockout and that endogenous iron accumulation leads to high-turnover type osteoporosis. Importantly,

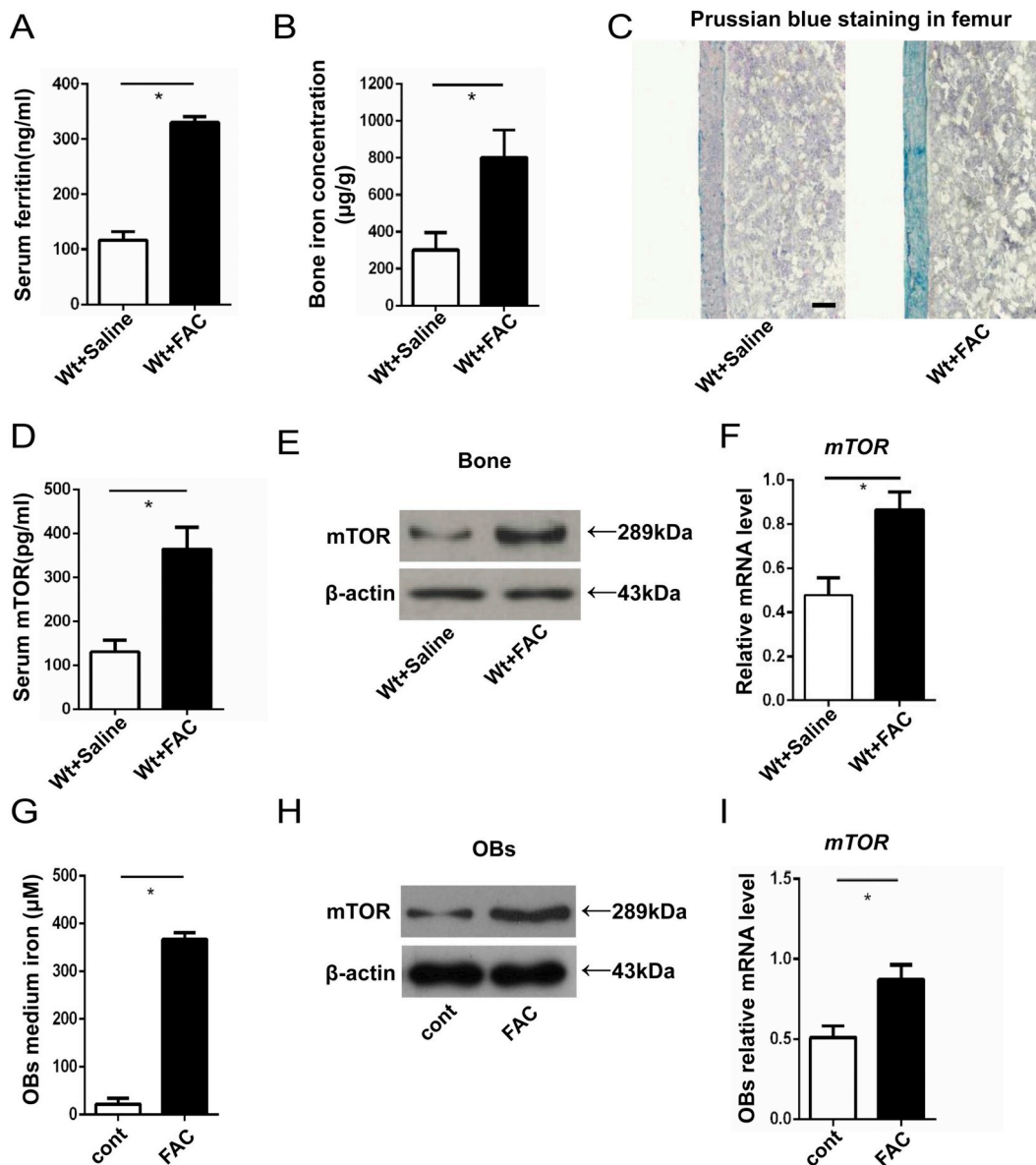


Fig. 1. Iron accumulation upregulates osteoblastic mTOR. (A) Concentration of serum ferritin as assessed by ELISA (n = 10 per group). (B) Iron concentration in femur of wild-type and FAC-treated male mice (n = 10 per group). (C) Representative images of Prussian blue staining in femur. Scale bar, 500 µm, (n = 10 per group). (D) Concentration of serum mTOR as assessed by ELISA (n = 10 per group). (E) Western blot of mTOR in tibia. (F) Quantitative PCR analysis of mTOR mRNA in tibia. (G) Iron concentration in culture medium of osteoblasts. (H) Western blot of mTOR in osteoblasts. (I) Quantitative PCR analysis of mTOR mRNA in osteoblasts. Data are shown as the mean ± s.d. *P < 0.05 (Student's *t*-test).

Hepc^{-/-} mice with ovariectomy exhibited increased serum levels of mTOR as well as enhanced mTOR protein and mRNA expression in bone (Fig. 2F–H). Thus, endogenous iron accumulation activates mTOR in bone of high-turnover type osteoporosis and aggravates high-turnover type osteoporosis.

3.3. Rapamycin improves bone in high-turnover osteoporosis with iron accumulation

Rapamycin is a common inhibitor of mTOR as it effectively suppresses the function of mTOR [36]. To evaluate the role of mTOR in the aggravation of high-turnover osteoporosis induced by iron accumulation, rapamycin was intraperitoneally injected into ovariectomized Hepc^{-/-} mice. Micro-CT analysis of cancellous bone showed that ovariectomized Hepc^{-/-} mice had poorer trabecular bone quality than ovariectomized Wt mice. Interestingly, the trabecular bone of ovariectomized Hepc^{-/-} mice injected with rapamycin showed partial

recovery compared to mice injected with CMC (Fig. 3A). BMD was significantly decreased in ovariectomized Hepc^{-/-} mice but was partially recovered with rapamycin injection (Fig. 3B). Other measured parameters, namely, BV/TV, TB.N, TB.Th, and ConnD, showed similar results to the BMD detection results (Fig. 3B). However, cortical bone measurements did not show distinct differences (Supplementary Fig. 3). To confirm if the bone deterioration of ovariectomized Hepc^{-/-} mice was recovered by rapamycin injection, mouse tibias were further analysed by HE staining, scanning electron microscopy (SEM) and biomechanical tests in different groups. HE staining and SEM showed that the amount of bone trabecula was markedly increased by rapamycin injection in ovariectomized Hepc^{-/-} mice, and the osteoblasts stained with ALP were increased too (Fig. 3C–D), but the osteoclasts stained with TRAP didn't vary significantly after rapamycin injection (Supplementary Fig. 4). The biomechanical tests demonstrated the recovery of bending modulus of elasticity, bending energy, maximum bending stress and bending rigidity coefficient after rapamycin injection

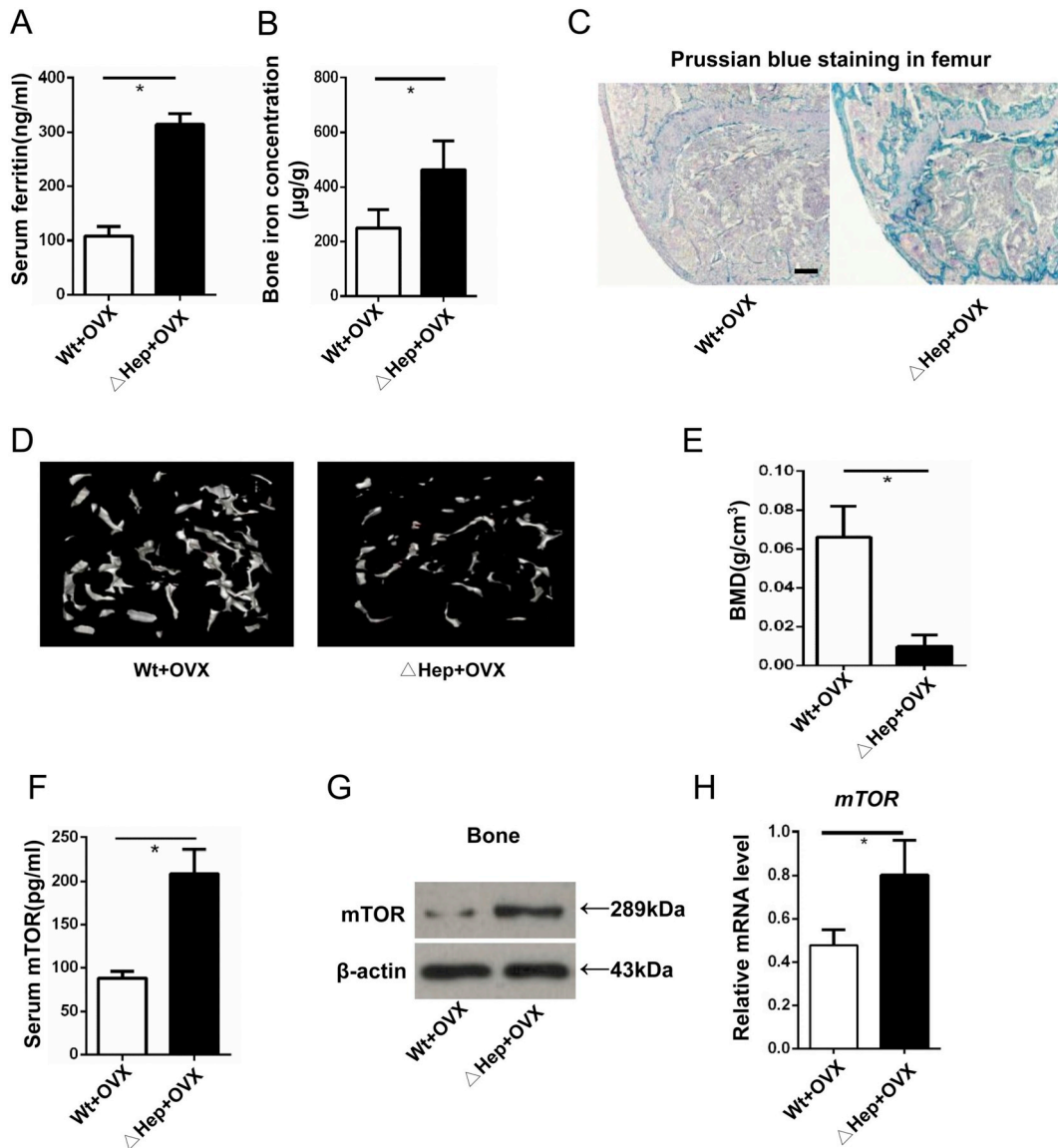


Fig. 2. Endogenous iron accumulation activates mTOR in high-turnover osteoporosis. (A) Concentration of serum ferritin as assessed by ELISA (n = 10 per group). (B) Iron concentration in femur of wild type and Hep^{-/-} mice with OVX (n = 10 per group). (C) Representative images of Prussian blue staining in femur. Scale bar, 500 μm, (n = 10 per group). (D) Representative images of Micro-CT in femur. (E) BMD analysis of femur of wild type and Hep^{-/-} mice with OVX (n = 10 per group). (F) Concentration of serum mTOR as assessed by ELISA (n = 10 per group). (G) Western blot of mTOR in tibia. (H) Quantitative PCR analysis of mTOR mRNA in tibia. Data are shown as the mean ± s.d. *P < 0.05 (Student's *t*-test).

(Fig. 3E). Together, these data suggested that iron accumulation accelerates bone loss in high-turnover osteoporosis and that increased mTOR level plays a key role in this process. Further, these data demonstrated that rapamycin ameliorates impaired bone mass and quality in high-turnover osteoporosis with iron accumulation.

3.4. Rapamycin ameliorates osteogenesis of high-turnover osteoporosis with iron accumulation

According to above findings, rapamycin improves the bone mass of high-turnover osteoporosis with iron accumulation. To determine if osteogenesis is ameliorated by rapamycin in high-turnover type osteoporosis with iron accumulation, the serum levels of ALP, PINP and Osteocalcin were measured to detect the activity of osteogenesis. All of these indicators were detected in the four groups of mice. These indicators were all sharply reduced in ovariectomized Hepc^{-/-} mice compared to ovariectomized Wt mice, and the levels were partially recovered in ovariectomized Hepc^{-/-} mice with rapamycin injection

(Fig. 4A). To confirm the change of osteogenesis, the mRNA expression of osteogenic genes, including SP7, Runx2 and OCN, was measured. The mRNA expression levels were consistent with the levels measured via ELISA (Fig. 4B). These observations revealed the improvement of bone mass accompanied by the ameliorated osteogenesis in ovariectomized Hepc^{-/-} mice with rapamycin injection.

For in vitro experiments, osteoblasts were transfected with mTOR-specific siRNAs to downregulate mTOR in osteoblasts, and mTOR suppression was verified (Supplementary Fig. 5). siRNA-transfected osteoblasts were then treated with FAC. As expected, the ALP staining of osteoblasts showed decreased alkaline activity in osteoblasts treated with FAC (Group.iron) compared to control (Group.cont), but transfection of mTOR siRNA (Group.iron + siR-MT) reversed the FAC-induced decrease in alkaline activity in compared to the negative control siRNA transfection group (Group.iron + siR-NC) (Fig. 4C). Mineralization of osteoblasts was measured by Alizarin Red staining, which agreed with the ALP staining (Fig. 4D). Furthermore, Runx2 and osteocalcin protein expression was significantly downregulated after FAC treatment

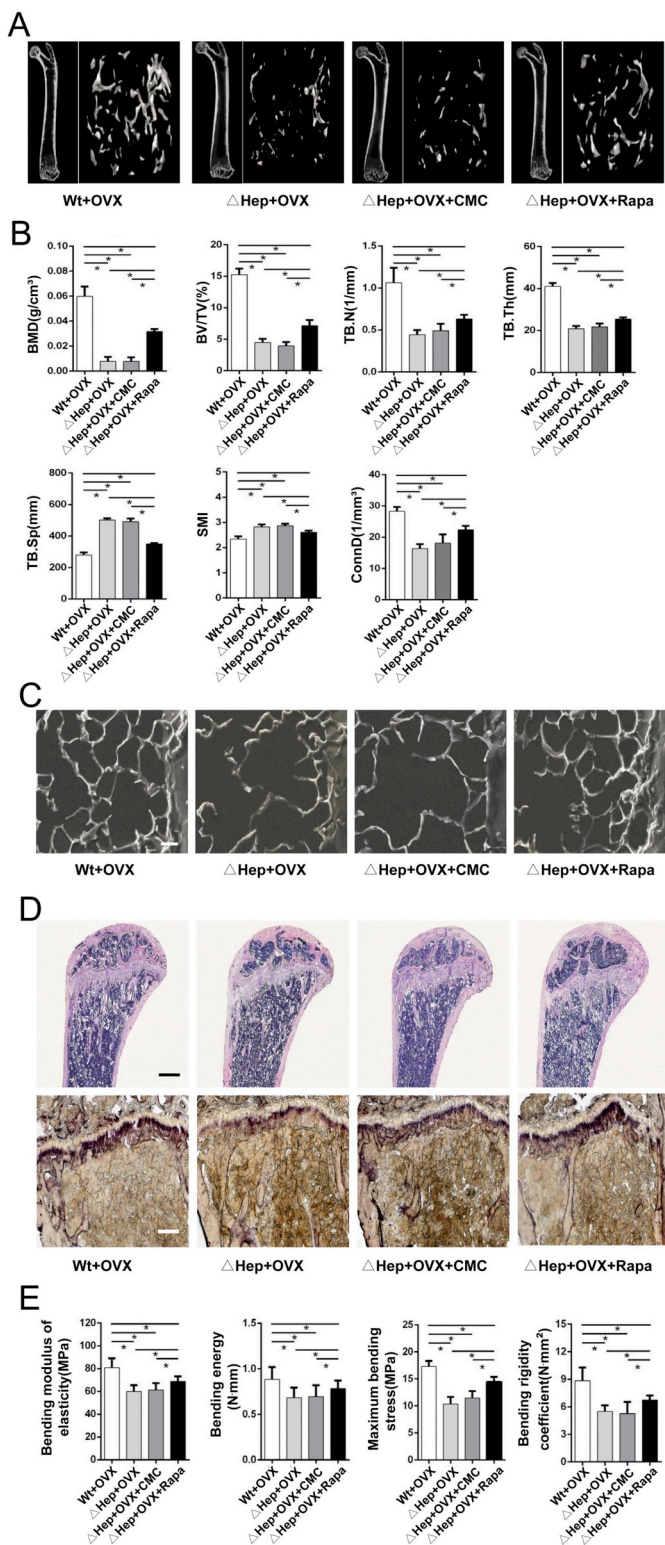


Fig. 3. Rapamycin improves bone of high-turnover osteoporosis with iron accumulation. (A) Representative images of Micro-CT in distal femur of ovariectomized wild type, Hep^{-/-} and rapamycin- or CMC-treated Hep^{-/-} mice (n = 8 per group). (B) Analyses of BMD and related trabecular parameters (BV/TV, TB.N, TB.Th, TB.Sp, SMI and ConnD) of femurs in four groups (n = 8 per group). (C) Representative SEM images of femurs. Scale bar, 50 μm. (D) Representative images of H&E and ALP staining of tibia. Scale bar, 500 μm, 1250 μm. (E) Biomechanical test analyses (bending modulus of elasticity, bending energy, maximum bending stress and bending rigidity coefficient) of femurs (n = 8 per group). Data are shown as the mean ± s.d. *P < 0.05 (One-way ANOVA test).

of osteoblasts, and the expression was partially recovered with transfection of mTOR siRNA (Fig. 4E). Similar results were obtained for the expression of Runx2, ALP and SP7 mRNA (Fig. 4F), indicating that the osteogenic activity of osteoblasts treated with FAC was reversed by mTOR suppression. Together, these results suggested that iron accumulation suppresses osteogenesis in bone of high-turnover type osteoporosis and that the improvement of bone mass and quality of high-turnover type osteoporosis with iron accumulation partially attributes to the amelioration of osteogenesis by rapamycin.

3.5. Rapamycin improves angiogenesis in high-turnover osteoporosis with iron accumulation

Given that osteogenesis and angiogenesis are tightly related in bone and that mTOR plays a key role in the crosstalk between osteogenesis and angiogenesis, the role of rapamycin in angiogenesis of high-turnover osteoporosis with iron accumulation was investigated by measuring the CD31 + Endomucin+ tibia vessels by immunostaining. These specific vessels have been reported to couple angiogenesis and osteogenesis in bone. Compared to ovariectomized wild type mice, a decrease of these specific vessels in tibia of ovariectomized Hepc^{-/-} mice was observed. Importantly, the amounts of specific vessels increased in ovariectomized Hepc^{-/-} mice with rapamycin injection compared to ovariectomized Hepc^{-/-} mice with CMC injection (Fig. 5A), and the level of slit3 which was related with this vessel tightly in groups showed consistent results (Fig. 5B), suggesting that rapamycin promotes bone vasculature formation in high-turnover osteoporosis with iron accumulation.

For in vitro experiments, HUVECs were cultured with corresponding medium (CM) extracted from treated osteoblasts. HUVECs cultured in CM from Group.iron osteoblasts exhibited a lower migration than that in control CM (Group.cont), and migration of HUVECs cultured in CM from Group.iron + siR-NC osteoblasts showed no difference compared to that of Group.iron osteoblasts. In contrast, migration of HUVECs cultured in CM from Group.iron + siR-MT osteoblasts was significantly enhanced compared to that of Group.iron osteoblasts (Fig. 5C). In contrast to the anastomosis tubules formed on Matrigel by HUVECs in control CM (Group.cont), HUVECs maintained in CM from Group.iron and Group.iron + siR-NC osteoblasts formed small cellular nests. However, HUVECs seeded on Matrigel in the presence of CM from Group.iron + siR-MT osteoblasts formed branching and short tubules (Fig. 5D). Immunostaining of endomucin on HUVECs showed a similar result (Fig. 5E). Thus, these in vivo and in vitro observations suggested that iron accumulation inhibits angiogenesis in bone of high-turnover type osteoporosis and that rapamycin plays a positive role in angiogenesis of high-turnover osteoporosis with iron accumulation.

3.6. Iron accumulation impairs osteoporotic bone via the osteoblastic mTOR/STAT1/Cxcl9 pathway

Because iron accumulation activates mTOR and impairs osteogenesis and angiogenesis in bone of high-turnover type osteoporosis, rapamycin was intraperitoneally injected into ovariectomized Hepc^{-/-} mice to suppress the high mTOR levels, which partially rescued the bone loss caused by iron accumulation. As shown in Fig. 6A, the higher level of mTOR induced by iron accumulation was decreased by rapamycin injection, but the iron accumulation was not changed. Similar observations were found in vitro. These observations revealed the underlying mechanism that iron accumulation impairs the osteoporotic bone via osteoblastic mTOR.

VEGF is downstream of mTOR, and it binds with VEGFR2 (KDR) on the membrane of osteoblasts and HUVECs to promote osteogenesis and angiogenesis [37,38]. Therefore, protein and mRNA expression levels of mTOR and VEGF were measured in treated osteoblasts. VEGF was positively regulated by mTOR at both protein and mRNA levels (Fig. 6B–C), and VEGF was increased in FAC-treated osteoblasts. These

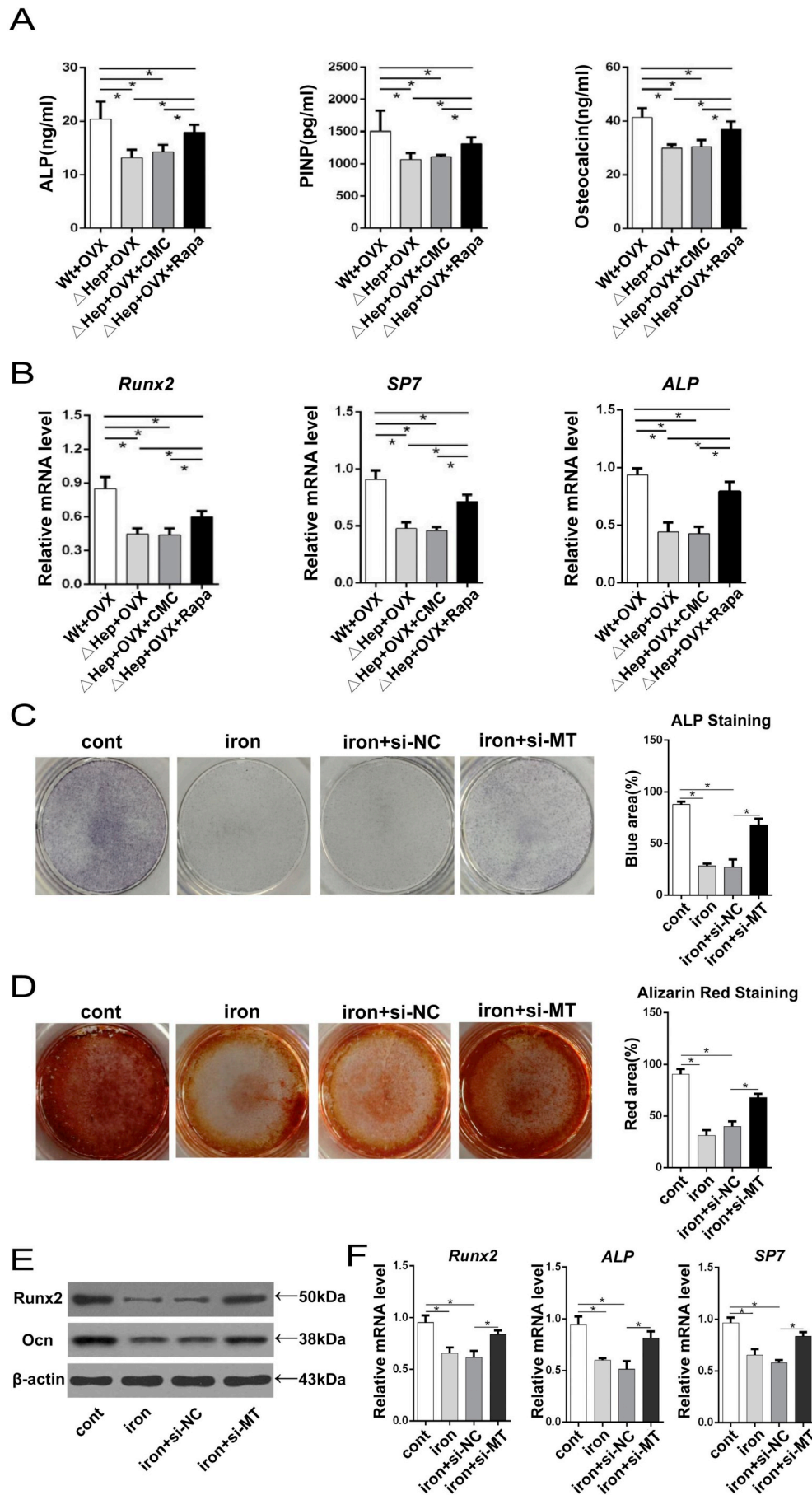


Fig. 4. Rapamycin ameliorates osteogenesis of high-turnover osteoporosis with iron accumulation. (A) Serum concentration of osteogenic proteins (ALP, P1NP and Osteocalcin) as assessed by ELISA (n = 8 per group). (B) Expression of osteogenic genes (Runx2, SP7 and ALP) in tibia were analysed by quantitative PCR. (C) Alkaline phosphatase staining of FAC-treated osteoblasts and FAC-treated osteoblasts transfected with negative control or mTOR siRNA. Quantitative analysis of blue staining compared to total area (n = 8 per group). (D) Alizarin staining of four osteoblast groups after culture for fourteen days (n = 8 per group). (E) Western blot of osteogenic proteins (Runx2 and Ocn) in four osteoblast groups. (F) Quantitative PCR analysis of osteogenic mRNA (Runx2, ALP and SP7) in four osteoblast groups. Data are shown as the mean \pm s.d. *P < 0.05, (One-way ANOVA). Abbreviations: si-NC, the group of osteoblasts transfected with negative control siRNA; si-MT, the group of osteoblasts transfected with mTOR siRNA.

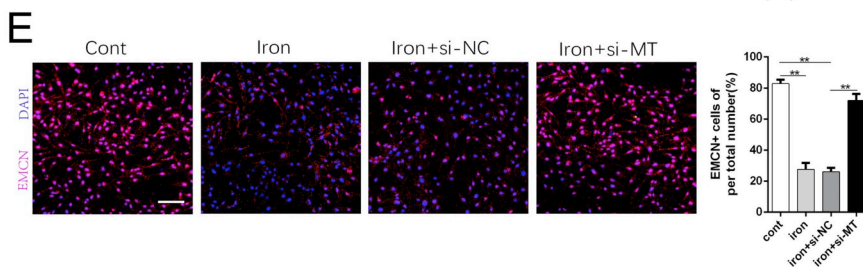
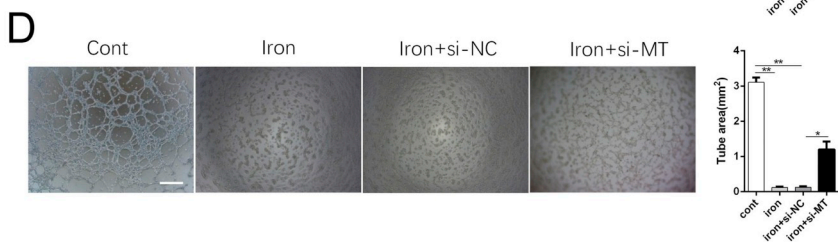
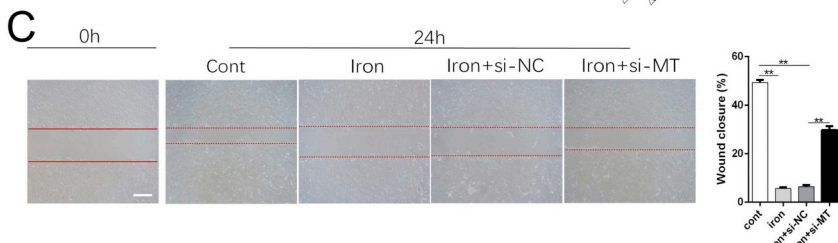
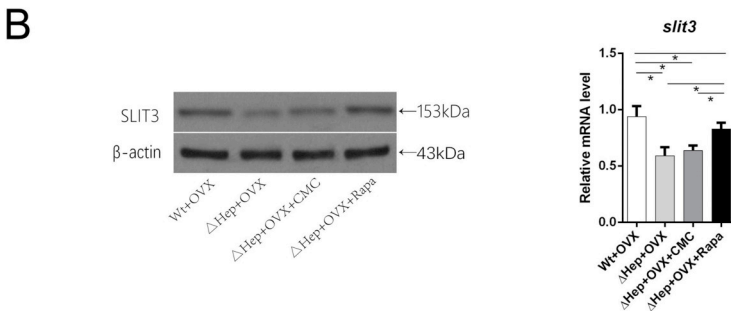
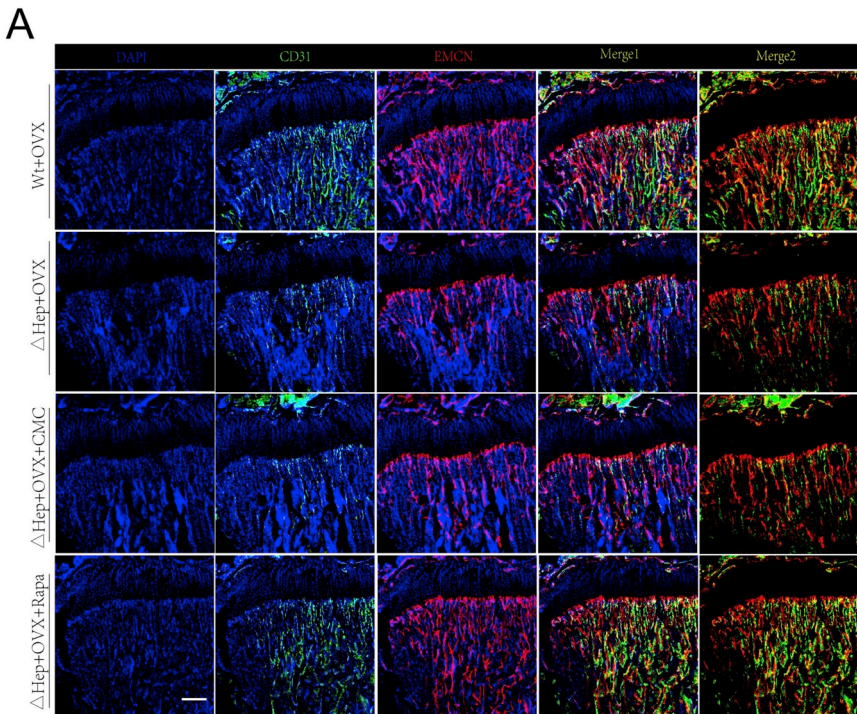


Fig. 5. Rapamycin improves angiogenesis of high-turn-over osteoporosis with iron accumulation. (A) Representative images of CD31 + EMCN+ microvessels in tibia sections of mice in the four groups. Scale bar, 200 μm. (B) Western blot of angiogenesis related protein slit3 and quantitative PCR analysis of mRNA slit3 in four groups. (C) Representative photomicrographs of wounds in HUVECs at 0 h and after 24 h. Dotted lines highlight the linear scratch/wound for each group of cells. Bar graph shows the mean percentage of wound closure. Scale bar, 500 μm. (n = 8 per group). (D) Representative photomicrographs of tube formation of HUVECs incubated with corresponding medium from osteoblasts on Matrigel, and quantitative analysis of tube area. Scale bar, 500 μm. (n = 8 per group). (E) Representative photomicrographs of immunostaining of EMCN in HUVECs cultured with corresponding medium from osteoblasts, and quantitative analysis of EMCN+ cells compared to total cells. Scale bar, 100 μm. Data are shown as the mean ± s.d. *P < 0.05, (One-way ANOVA).

Abbreviations: si-NC, HUVECs cultured with medium extracted from osteoblasts transfected with negative control siRNA; si-MT, HUVECs cultured with medium extracted from osteoblasts transfected with mTOR siRNA.

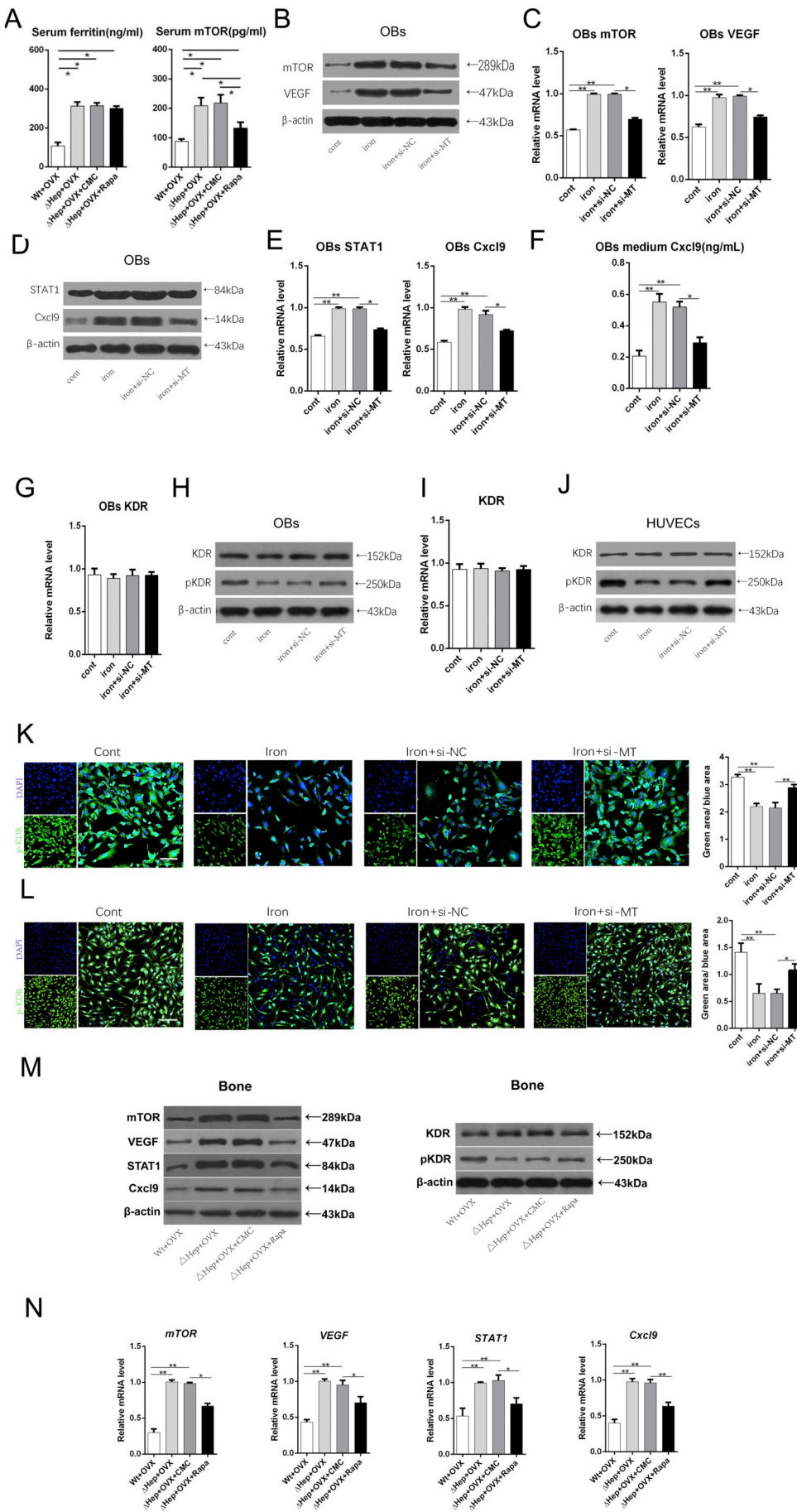


Fig. 6. Gene and protein expression of the osteoblastic mTOR/STAT1/Cxcl9 pathway molecules. (A) Serum ferritin and mTOR concentration in Wt + OVX, Δ Hep + OVX, Δ Hep + OVX + CMC and Δ Hep + OVX + Rapa mice (n = 8 per group). (B) Western blot of mTOR and VEGF protein in cont, iron, iron + si-NC and iron + si-MT group osteoblasts. (C) Quantitative PCR analysis of mTOR and VEGF in four osteoblast groups. (D) Protein expression of STAT1 and Cxcl9 as assessed by western blot in differently treated osteoblasts. (E) mRNA expression of STAT1 and Cxcl9 as measured by Q-PCR in osteoblasts. (F) Cxcl9 concentration in culture medium of osteoblasts (n = 8 per group). (G) KDR gene expression in osteoblasts as assessed by Q-PCR. (H) KDR and p-KDR protein expression in osteoblasts assessed by western blot. (I) Quantitative analysis of KDR in HUVECs cultured with corresponding medium from osteoblasts. (J) Western blot of KDR and p-KDR in HUVECs. (K) Representative images of osteoblasts immunostained by p-KDR, and quantitative analysis of green area compared to blue area. Scale bar, 100 μ m. (L) Representative images of HUVECs immunostained by p-KDR, and quantitative analysis of green area compared to blue area. Scale bar, 100 μ m. (M) Western blot of mechanism proteins in four group mice's bone. (N) Quantitative PCR analysis of mechanism mRNA in four mice groups. Data are shown as the mean \pm s.d. *P < 0.05, (One-way ANOVA). (For interpretation of the references to color in this figure legend, the reader is referred to the web version of this article.)

changes did not account for the osteogenesis and angiogenesis alterations in bone and in vivo, suggesting that osteoblasts may secrete another VEGF-related inhibitory factor.

Cxcl9 interacts with VEGF to prevent VEGF from binding to VEGFR2 [39]. Moreover, mTOR regulates Cxcl9 in osteoblasts via STAT1 [40]. The expression and secretion of Cxcl9 protein and mRNA were positively regulated by mTOR in osteoblasts (Fig. 6D–F). The changes in STAT1 protein and mRNA were consistent with the changes in mTOR in osteoblasts (Fig. 6D–E), indicating that the higher mTOR levels induced by iron accumulation upregulate Cxcl9 secretion in osteoblasts.

To confirm the Cxcl9-induced prevention of binding, KDR mRNA and protein expression level were measured in osteoblasts and HUVECs, and there was no significant differences among the groups (Fig. 6G–J). Moreover, the phosphorylation of KDR was decreased in FAC-treated osteoblasts and HUVECs cultured in CM, and the phosphorylation of KDR was reversed in Group.iron + siR-MT osteoblasts and HUVECs cultured in CM (Fig. 6H, J). Immunostaining of p-KDR in osteoblasts and HUVECs showed similar results (Fig. 6K–L), and all these varieties were verified in bones of mouse models (Fig. 6M–N), indicating that increased secretion of Cxcl9 prevented the binding between VEGF and KDR to inhibit activity of osteoblasts and HUVECs. Further, the binding prevention was alleviated when Cxcl9 secretion was decreased by mTOR suppression. Together, these results suggested that iron accumulation impairs osteogenesis and angiogenesis in osteoporotic bone via the osteoblastic mTOR/STAT1/Cxcl9 pathway (Fig. 7).

4. Discussion

The present study showed that iron accumulation activates osteoblastic mTOR both in mouse models of iron accumulation and mouse models of high-turnover type osteoporosis with endogenous iron accumulation. Moreover, rapamycin (an inhibitor of mTOR) was shown to have a positive role in the improvement of bone mass in high-turnover type osteoporosis with iron accumulation. Rapamycin decreased Cxcl9

secretion by suppressing mTOR in osteoblasts, which inhibited VEGF binding to its receptor by interacting with VEGF, leading to the promotion of osteogenesis and angiogenesis. Thus, rapamycin promotes osteogenesis and angiogenesis to improve the bone mass of high-turnover type osteoporosis with iron accumulation.

Osteoporosis often occurs in postmenopausal women, in which it is identified as type I osteoporosis, and it maintains a high-bone turnover state [41,42]. Menopause is usually accompanied with iron accumulation and bone loss, and serum ferritin has a negative relationship with BMD in postmenopausal women [15,43]. In addition, the level of mTOR is tightly associated with iron and osteoporosis. Iron deficiency inhibits the activation of mTOR in intestinal cells, and mTOR induces osteoclasts to decrease bone mass [44,45]. A previous study reported, inactivation of regulatory-associated protein of mTOR signalling in osteoclasts of conditional Raptor knockout mice significantly increases bone mass, for osteoclast differentiation of Raptor-deficient bone marrow macrophages (BMMs) is impaired. The most likely explanation for this phenomenon is mTOR activation leads to a simultaneous increase in RANKL and decrease in OPG expression, increase of RANKL expression is requisite for osteoclast differentiation and OPG can inhibit bone resorption of osteoclasts [46]. There were also some researches about mTOR in osteoblasts, but the role of mTOR and rapamycin (include other mTOR inhibitors) on osteoblasts and osteoclasts were still a long-standing debate. HoangDinh Huynh found that rapamycin has a negative effect on bone mass [47], however, Meng Qi etc. discovered that rapamycin can increase bone mass of estrogen-deficient mice [48], an appropriate level of mTOR may account for the different results, neither too high or too low level of mTOR has benefit on bone mass. In addition, different mouse models may also display various effects of rapamycin, and it's all same to different ramifications of rapamycin, such as temsirolimus, everolimus, Deforolimus and so on, this may be explained by different proficiency and mechanisms of them [49,50]. Since the osteoporosis with iron accumulation mainly occurs in postmenopausal women and no significant variety of mTOR was detected in

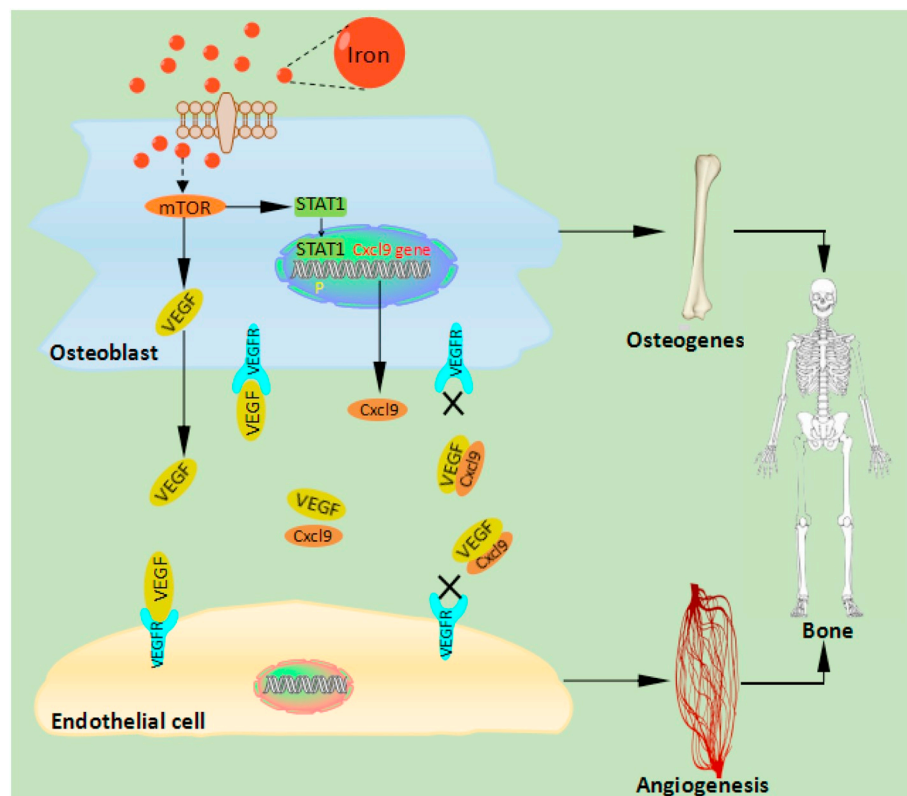


Fig. 7. Model of iron accumulation impairment of osteogenesis and angiogenesis in bone. Iron accumulation activates mTOR and downstream STAT1 in osteoblasts, increasing the secretion of Cxcl9 in osteoblasts and binding with VEGF. VEGF binding leads to inactivation of receptor on osteoblasts and HUVECs, thereby inhibiting osteogenesis and angiogenesis in bone.

iron treated osteoclasts (Supplementary Fig. 6), our experiments mostly focused on osteoblastic mTOR in mouse models of high-turnover osteoporosis with iron accumulation.

For the first time, the present study detected the level of osteoblastic mTOR in mouse models with iron accumulation and in mouse models of high-turnover osteoporosis with iron accumulation. Considering that iron homeostasis can fluctuate by exogenous injection of medication, transgenic mice (Hep^{-/-}) were used to establish mouse models of high-turnover osteoporosis with iron accumulation [51]. As expected, iron accumulation activates mTOR, both rapamycin and other mTOR inhibitors may benefit the bone of transgenic mice (Hep^{-/-}) directly, but the underlying mechanism is not fully elucidated.

Both the activation of osteoblasts and generation of blood vessels are essential to maintain bone homeostasis [6,52]. Enhanced differentiation of osteoblasts and increased proliferation of osteoblasts significantly increase the bone mass of mice, and abundant bone vessels can accelerate bone regeneration and healing of bone fracture [53,54]. Therefore, the improvement of bone mass is related to osteogenesis and angiogenesis, and healthy mice with endogenous iron accumulation shows decreased volume of bone and blood vessels (Supplementary Fig. 7). Rapamycin significantly promotes differentiation of osteoblasts and inhibits differentiation of osteoclasts, thereby playing an important role in bone protection [55]. However, the role of rapamycin in bone vessels is not fully known. Rapamycin, an effective inhibitor of mTOR, was injected into the mouse models of high-turnover osteoporosis with iron accumulation to demonstrate the role of rapamycin in bone loss related to iron accumulation. Both the osteogenesis and angiogenesis were observed in bone and in vitro in the four groups. Interestingly, the bone mass of mouse models injected with rapamycin was increased, and effective inhibition of mTOR ameliorated the osteogenesis and angiogenesis in bone of high-turnover type osteoporosis with iron accumulation. Because rapamycin mainly targets mTORC1, it remains unclear if mTORC2 plays a part in this process. Future studies should address the involvement of mTORC2 in this process.

The deteriorated bone mass, osteogenesis and angiogenesis of high-turnover type osteoporosis with iron accumulation were all improved by injection of rapamycin. These improvements mostly were detected in cancellous bone instead of cortical bone, because cancellous bone mainly reflects the state of bone metabolism and changed with bone metabolism timely, in comparison, cortical bone indicates station of skeleton development, it's stable and varied with aging slowly. In this process, higher mTOR activated by iron accumulation was suppressed successfully, but the state of iron accumulation still existed, suggesting that mTOR plays a key role in the bone loss of high-turnover type osteoporosis with iron accumulation. In the present study, the expression of VEGF, which is known to play a role in the crosstalk between osteogenesis and angiogenesis, was measured. However, the results did not account for the corresponding alteration of osteogenesis and angiogenesis. Cxcl9 has been reported to be constitutively expressed in osteoblasts and that Cxcl9 expression is positively regulated by mTOR upstream of STAT1. Cxcl9 inhibits blood vessel formation and osteogenesis by interacting with VEGF, thereby preventing its binding to HUVECs and osteoblasts [31]. Consistently, the present study showed that the expression of Cxcl9 was positively regulated by mTOR via STAT1 and that increased Cxcl9 expression suppressed the phosphorylation of KDR (receptor of VEGF) on HUVECs and osteoblasts.

5. Conclusions

In summary, the present study identified the key role of mTOR in high-turnover osteoporosis with iron accumulation. Iron accumulation impairs the bone regeneration of osteoporosis via the osteoblastic mTOR/STAT1/Cxcl9 pathway. Rapamycin targets mTOR, thereby improving osteogenesis and angiogenesis in bone of high-turnover type osteoporosis with iron accumulation, which increases bone mass.

Therefore, rapamycin may be an effective therapeutic strategy for type I osteoporosis with iron accumulation in human.

Supplementary data to this article can be found online at <https://doi.org/10.1016/j.bone.2018.12.019>.

Author contributions

J.W., X.W., Y.X. designed research; J.W., A.W. conducted the experiments and acquired data; J.W., A.W. analysed data and performed statistical analysis; J.W., A.W. wrote the manuscript; G.L., P.J., G.S., Y.Y., H.Z., F.Y. provided good suggestions during the study process and manuscript revising. All authors have approved the final article.

Acknowledgments

Sincere thanks to Wang Aifei for his help of laboratory work. We thank Xiao Wang, Ying Xu, Youjia Xu for helping with the design of the experiment.

Funding source

This work was supported by grants from the National Natural Science Foundation of China (No. 81874018 and 81803242), Pre-Research Fund of the National Natural Science Foundation of China (No. SDFEYJ1601), Postgraduate Research & Practice Innovation Program of Jiangsu Province (No. KYCX17_1996), Jiangsu Provincial Young Medical Talents Program (No. QNRC2016880), Suzhou Grant (No. SZZXJ201504 and SS201634), and Hospital preponderant academic subjects group (No. XKQ2015001), Jiangsu Natural Science Foundation (Youth Foundation) (No. BK2017095), Suzhou People's Livelihood Science and Technology Project (No. sys 2018053).

Conflicts of interest

All authors report no conflicts of interest.

References

- [1] S.C. DeShields, T.D. Cunningham, Comparison of osteoporosis in US adults with type 1 and type 2 diabetes mellitus, *J. Endocrinol. Investig.* (2018), <https://doi.org/10.1007/s40618-018-0828-x>.
- [2] E. Hernlund, A. Svedbom, M. Ivergard, et al., Osteoporosis in the European Union: medical management, epidemiology and economic burden. A report prepared in collaboration with the International Osteoporosis Foundation (IOF) and the European Federation of Pharmaceutical Industry Associations (EFPIA), *Arch. Osteoporos.* 8 (2013) 136, <https://doi.org/10.1007/s11657-013-0136-1>.
- [3] G. Karsenty, The complexities of skeletal biology, *Nature* 423 (6937) (2003) 316–318, <https://doi.org/10.1038/nature01654>.
- [4] J. Marx, Coming to grips with bone loss, *Science* 305 (5689) (2004) 1420–1422, <https://doi.org/10.1126/science.305.5689.1420>.
- [5] E. Schipani, C. Maes, G. Carmeliet, et al., Regulation of osteogenesis-angiogenesis coupling by HIFs and VEGF, *J. Bone Miner. Res.* 24 (8) (2009) 1347–1353, <https://doi.org/10.1359/Jbmr.090602>.
- [6] A.P. Kusumbe, S.K. Ramasamy, R.H. Adams, Coupling of angiogenesis and osteogenesis by a specific vessel subtype in bone, *Nature* 507 (7492) (2014) 323–328, <https://doi.org/10.1038/nature13145>.
- [7] M. Gambacciani, M. Levancini, Hormone replacement therapy and the prevention of postmenopausal osteoporosis, *Prz. Menopausalny* 13 (4) (2014) 213–220, <https://doi.org/10.5114/pm.2014.44996>.
- [8] A. Gupta, L. March, Treating osteoporosis, *Aust. Prescr.* 39 (2) (2016) 40–46, <https://doi.org/10.18773/austprescr.2016.028>.
- [9] G. Li, L. Thabane, A. Papaioannou, et al., An overview of osteoporosis and frailty in the elderly, *BMC Musculoskelet. Disord.* 18 (1) (2017) 46, <https://doi.org/10.1186/s12891-017-1403-x>.
- [10] Management of osteoporosis in postmenopausal women: 2010 position statement of The North American Menopause Society, *Menopause* 17 (1) (2010) 25–54, <https://doi.org/10.1097/gme.0b013e3181c617e6> (quiz 55–26).
- [11] A.M. Briggs, M.J. Cross, D.G. Hoy, et al., Musculoskeletal health conditions represent a global threat to healthy aging: a report for the 2015 World Health Organization World Report on Ageing and Health, *Gerontologist* 56 (Suppl. 2) (2016) S243–S255, <https://doi.org/10.1093/geront/gnw002>.
- [12] E.D. Weinberg, Role of iron in osteoporosis, *Pediatr. Endocrinol. Rev.* 6 (Suppl. 1) (2008) 81–85.

- [13] X. Wang, B. Chen, J. Sun, et al., Iron-induced oxidative stress stimulates osteoclast differentiation via NF-kappaB signaling pathway in mouse model, *Metabolism* 83 (2018) 167–176, <https://doi.org/10.1016/j.metabol.2018.01.005>.
- [14] C. Camaschella, Iron-deficiency anemia, *N. Engl. J. Med.* 373 (5) (2015) 485–486, <https://doi.org/10.1056/NEJMc1507104>.
- [15] B.J. Kim, S.H. Ahn, S.J. Bae, et al., Iron overload accelerates bone loss in healthy postmenopausal women and middle-aged men: a 3-year retrospective longitudinal study, *J. Bone Miner. Res.* 27 (11) (2012) 2279–2290, <https://doi.org/10.1002/jbmr.1692>.
- [16] B. Chen, G.F. Li, Y. Shen, et al., Reducing iron accumulation: a potential approach for the prevention and treatment of postmenopausal osteoporosis, *Exp. Ther. Med.* 10 (1) (2015) 7–11, <https://doi.org/10.3892/etm.2015.2484>.
- [17] V. Jeney, Clinical impact and cellular mechanisms of iron overload-associated bone loss, *Front. Pharmacol.* 8 (Pt 2) (2017) 77, <https://doi.org/10.3389/fphar.2017.00077>.
- [18] E. Balogh, E. Tolnai, B. Nagy Jr. et al., Iron overload inhibits osteogenic commitment and differentiation of mesenchymal stem cells via the induction of ferritin, *Biochim. Biophys. Acta* 1862 (9) (2016) 1640–1649, <https://doi.org/10.1016/j.bbdis.2016.06.003>.
- [19] L. Wang, F. Zhou, P. Zhang, et al., Human type H vessels are a sensitive biomarker of bone mass, *Cell Death Dis.* 8 (5) (2017) e2760, <https://doi.org/10.1038/cddis.2017.36>.
- [20] L. Wang, P. Jia, Y. Shan, et al., Synergistic protection of bone vasculature and bone mass by desferrioxamine in osteoporotic mice, *Mol. Med. Rep.* 16 (5) (2017) 6642–6649, <https://doi.org/10.3892/mmr.2017.7451>.
- [21] J. Drager, E.J. Harvey, J. Barralet, Hypoxia signalling manipulation for bone regeneration, *Expert Rev. Mol. Med.* 17 (2015) e6, <https://doi.org/10.1017/erm.2015.4>.
- [22] J. Drager, Z. Sheikh, Y.L. Zhang, et al., Local delivery of iron chelators reduces in vivo remodeling of a calcium phosphate bone graft substitute, *Acta Biomater.* 42 (2016) 411–419, <https://doi.org/10.1016/j.actbio.2016.07.037>.
- [23] C. Vezina, A. Kudelski, S.N. Sehgal, Rapamycin (AY-22,989), a new antifungal antibiotic. I. Taxonomy of the producing streptomycete and isolation of the active principle, *J. Antibiot. (Tokyo)* 28 (10) (1975) 721–726.
- [24] D.W. Lammung, L. Ye, P. Katajisto, et al., Rapamycin-induced insulin resistance is mediated by mTORC2 loss and uncoupled from longevity, *Science* 335 (6076) (2012) 1638–1643, <https://doi.org/10.1126/science.1215135>.
- [25] J.Q. Chen, F.X. Long, mTOR signaling in skeletal development and disease, *Bone Res.* 6 (1) (2018) 1, <https://doi.org/10.1038/s41413-017-0004-5>.
- [26] Y. Zhang, S. Xu, K. Li, et al., mTORC1 inhibits NF-kappa B/NFATc1 signaling and prevents osteoclast precursor differentiation, in vitro and in mice, *J. Bone Miner. Res.* 32 (9) (2017) 1829–1840, <https://doi.org/10.1002/jbmr.3172>.
- [27] J. Chen, X. Tu, E. Esen, et al., WNT7B Promotes Bone Formation in part through mTORC1, *PLoS Genet.* 10 (1) (2014) e1004145, <https://doi.org/10.1371/journal.pgen.1004145>.
- [28] C.M. Karner, S.Y. Lee, F. Long, Bmp induces osteoblast differentiation through both Smad4 and mTORC1 signaling, *Mol. Cell. Biol.* 37 (4) (2017), <https://doi.org/10.1128/MCB.00253-16> (e00253-00216).
- [29] P. Hadji, R. Coleman, M. Gnant, Bone effects of mammalian target of rapamycin (mTOR) inhibition with everolimus, *Crit. Rev. Oncol. Hematol.* 87 (2) (2013) 101–111, <https://doi.org/10.1016/j.critrevonc.2013.05.015>.
- [30] A.J. Browne, M.L. Kubasch, A. Gobel, et al., Concurrent antitumor and bone-protective effects of everolimus in osteotropic breast cancer, *Breast Cancer Res.* 19 (1) (2017) 92, <https://doi.org/10.1186/s13058-017-0885-7>.
- [31] B. Huang, W.H. Wang, Q.C. Li, et al., Osteoblasts secrete Cxcl9 to regulate angiogenesis in bone, *Nat. Commun.* 7 (2016) 13885, <https://doi.org/10.1038/ncomms13885>.
- [32] P. Jia, Y.J. Xu, Z.L. Zhang, et al., Ferric ion could facilitate osteoclast differentiation and bone resorption through the production of reactive oxygen species, *J. Orthop. Res.* 30 (11) (2012) 1843–1852, <https://doi.org/10.1002/jor.22133>.
- [33] R. Paddenberg, P. Stieger, A.L. von Lilien, et al., Rapamycin attenuates hypoxia-induced pulmonary vascular remodeling and right ventricular hypertrophy in mice, *Respir. Res.* 8 (1) (2007) 15, <https://doi.org/10.1186/1465-9921-8-15>.
- [34] M.P. Akhter, D.M. Cullen, G. Gong, et al., Bone biomechanical properties in prostaglandin EP1 and EP2 knockout mice, *Bone* 29 (2) (2001) 121–125, [https://doi.org/10.1016/S8756-3282\(01\)00486-0](https://doi.org/10.1016/S8756-3282(01)00486-0).
- [35] J.G. Messer, A.K. Kilbarger, K.M. Erikson, et al., Iron overload alters iron-regulatory genes and proteins, down-regulates osteoblastic phenotype, and is associated with apoptosis in fetal rat calvaria cultures, *Bone* 45 (5) (2009) 972–979, <https://doi.org/10.1016/j.bone.2009.07.073>.
- [36] R.A. Saxton, D.M. Sabatini, mTOR signaling in growth, metabolism, and disease (vol 168, pg 960, 2017), *Cell* 169 (2) (2017) 361–371, <https://doi.org/10.1016/j.cell.2017.03.035>.
- [37] S. Koch, L. Claesson-Welsh, Signal transduction by vascular endothelial growth factor receptors, *Cold Spring Harb. Perspect. Med.* 2 (7) (2012) a006502, <https://doi.org/10.1101/cshperspect.a006502>.
- [38] C.T. Chen, Y. Du, H. Yamaguchi, et al., Targeting the IKK beta/mTOR/VEGF signaling pathway as a potential therapeutic strategy for obesity-related breast cancer, *Mol. Cancer Ther.* 11 (10) (2012) 2212–2221, <https://doi.org/10.1158/1535-7163.Mct-12-0180>.
- [39] H. Sahin, E. Borkham-Kamphorst, C. Kuppe, et al., Chemokine Cxcl9 attenuates liver fibrosis-associated angiogenesis in mice, *Hepatology* 55 (5) (2012) 1610–1619, <https://doi.org/10.1002/hep.25545>.
- [40] S. Bruneau, H. Nakayama, C.B. Woda, et al., DEPTOR regulates vascular endothelial cell activation and proinflammatory and angiogenic responses, *Blood* 122 (10) (2013) 1833–1842, <https://doi.org/10.1182/blood-2013-03-488486>.
- [41] R. Eastell, S.P. Robins, T. Colwell, et al., Evaluation of bone turnover in type-I osteoporosis using biochemical markers specific for both bone-formation and bone-resorption, *Osteoporos. Int.* 3 (5) (1993) 255–260, <https://doi.org/10.1007/Bf01623829>.
- [42] D.M. Black, C.J. Rosen, Clinical practice. Postmenopausal osteoporosis, *N. Engl. J. Med.* 374 (3) (2016) 254–262, <https://doi.org/10.1056/NEJMc1513724>.
- [43] B.J. Kim, S.H. Lee, J.M. Koh, et al., The association between higher serum ferritin level and lower bone mineral density is prominent in women >= 45 years of age (KNHANES 2008–2010), *Osteoporos. Int.* 24 (10) (2013) 2627–2637, <https://doi.org/10.1007/s00198-013-2363-0>.
- [44] A. Watson, C. Lipina, H.J. McArdle, et al., Iron depletion suppresses mTORC1-directed signalling in intestinal Caco-2 cells via induction of REDD1, *Cell. Signal.* 28 (5) (2016) 412–424, <https://doi.org/10.1016/j.cellsig.2016.01.014>.
- [45] S. Xu, Y. Zhang, B. Liu, et al., Activation of mTORC1 in B lymphocytes promotes osteoclast formation via regulation of beta-catenin and RANKL/OPG, *J. Bone Miner. Res.* 31 (7) (2016) 1320–1333, <https://doi.org/10.1002/jbmr.2800>.
- [46] Q. Dai, F. Xie, Y. Han, et al., Inactivation of regulatory-associated protein of mTOR (rapTOR)/mammalian target of rapamycin complex 1 (mTORC1) signaling in osteoclasts increases bone mass by inhibiting osteoclast differentiation in mice, *J. Biol. Chem.* 292 (1) (2017) 196–204, <https://doi.org/10.1074/jbc.M116.764761>.
- [47] H. Huynh, Y. Wan, mTORC1 impedes osteoclast differentiation via calcineurin and NFATc1, *Commun. Biol.* 1 (2018) 29, <https://doi.org/10.1038/s42003-018-0028-4>.
- [48] M. Qi, L. Zhang, Y. Ma, et al., Autophagy maintains the function of bone marrow mesenchymal stem cells to prevent estrogen deficiency-induced osteoporosis, *Theranostics* 7 (18) (2017) 4498–4516, <https://doi.org/10.7150/thno.17949>.
- [49] S. Mukhopadhyay, M.A. Frias, A. Chatterjee, et al., The enigma of rapamycin dosage, *Mol. Cancer Ther.* 15 (3) (2016) 347–353, <https://doi.org/10.1158/1535-7163.MCT-15-0720>.
- [50] P.J. Houghton, Everolimus, *Clin. Cancer Res.* 16 (5) (2010) 1368–1372, <https://doi.org/10.1158/1078-0432.CCR-09-1314>.
- [51] S. Granick, *Iron Metabolism*, *Bull. N. Y. Acad. Med.* 30 (2) (1954) 81–105.
- [52] F. Xiao, C.D. Wang, C.L. Wang, et al., BMPER enhances bone formation by promoting the osteogenesis-angiogenesis coupling process in mesenchymal stem cells, *Cell. Physiol. Biochem.* 45 (5) (2018) 1927–1939, <https://doi.org/10.1159/000487969>.
- [53] A. Grosso, M. Burger, A. Lunger, et al., It takes two to tango: coupling of angiogenesis and osteogenesis for bone regeneration, *Front. Bioeng. Biotechnol.* 5 (2017) 68, <https://doi.org/10.3389/fbioe.2017.00068>.
- [54] E.C. Hsiao, B.M. Boudignon, W.C. Chang, et al., Osteoblast expression of an engineered G(s)-coupled receptor dramatically increases bone mass, *Proc. Natl. Acad. Sci. U. S. A.* 105 (4) (2008) 1209–1214, <https://doi.org/10.1073/pnas.0707457105>.
- [55] K.W. Lee, J.Y. Yook, M.Y. Son, et al., Rapamycin promotes the osteoblastic differentiation of human embryonic stem cells by blocking the mTOR pathway and stimulating the BMP/Smad pathway, *Stem Cells Dev.* 19 (4) (2010) 557–568, <https://doi.org/10.1089/scd.2009.0147>.